

## Three-Dimensional Relationships Between Perisynaptic Astroglia and Human Hippocampal Synapses

MARK R. WITCHER,<sup>1</sup> YONG D. PARK,<sup>2</sup> MARK R. LEE,<sup>3</sup> SUASH SHARMA,<sup>4</sup> KRISTEN M. HARRIS,<sup>2,5\*</sup> AND SERGEI A. KIROV<sup>3\*</sup>

<sup>1</sup>MD/PhD Program, Medical College of Georgia, Augusta, Georgia

<sup>2</sup>Department of Neurology, Medical College of Georgia, Augusta, Georgia

<sup>3</sup>Department of Neurosurgery, Medical College of Georgia, Augusta, Georgia

<sup>4</sup>Department of Pathology, Medical College of Georgia, Augusta, Georgia

<sup>5</sup>Center for Learning and Memory and Section of Neurobiology, The University of Texas, Austin, Texas

### KEY WORDS

tripartite synapse; epilepsy; seizures; astrogliosis; dendritic spines; stereology

### ABSTRACT

Perisynaptic astroglia are critical for normal synaptic development and function. Little is known, however, about perisynaptic astroglia in the human hippocampus. When mesial temporal lobe epilepsy (MTLE) is refractory to medication, surgical removal is required for seizure quiescence. To investigate perisynaptic astroglia in human hippocampus, we recovered slices for several hours *in vitro* from three surgical specimens and then quickly fixed them to achieve high-quality ultrastructure. Histological samples from each case were found to have mesial temporal sclerosis with Blumcke Type 1a (mild, moderate) or 1b (severe) pathology. Quantitative analysis through serial section transmission electron microscopy in CA1 *stratum radiatum* revealed more synapses in the mild (10/10  $\mu\text{m}^3$ ) than the moderate (5/10  $\mu\text{m}^3$ ) or severe (1/10  $\mu\text{m}^3$ ) cases. Normal spines occurred in mild and moderate cases, but a few multisynaptic spines were all that remained in the severe case. Like adult rat hippocampus, perisynaptic astroglial processes were preferentially associated with larger synapses in the mild and moderate cases, but rarely penetrated the cluster of axonal boutons surrounding multisynaptic spines. Synapse perimeters were only partially surrounded by astroglial processes such that all synapses had some access to substances in the extracellular space, similar to adult rat hippocampus. Junctions between astroglial processes were observed more frequently in moderate than mild case, but were obscured by densely packed intermediate filaments in astroglial processes of the severe case. These findings suggest that perisynaptic astroglial processes associate with synapses in human hippocampus in a manner similar to model systems and are disrupted by severe MTLE pathology. ©2009 Wiley-Liss, Inc.

### INTRODUCTION

Astroglial processes normally provide neuroprotection (Rosenberg and Aizenman, 1989), enhance synapse efficacy and maturation (Hama et al., 2004; Mazzanti and Haydon, 2003; Murai et al., 2003; Pfrieger and Barres, 1997), and mediate selective synapse elimination (Stevens et al., 2007). Hippocampal perisynaptic astroglial processes are associated with larger synapses, but newly formed or small synapses have little or none (Witcher

et al., 2007). Epilepsy affects ~50 million people worldwide, and mesial temporal lobe epilepsy (MTLE) is among the most prevalent and most refractory to medical treatment (Spencer, 2002). Hence, surgically resected human hippocampus becomes available as a source of human brain tissue for experimental analysis. Loss of neurons and dendritic spines and the formation of varicose dendritic shafts have been associated with seizures (Jiang et al., 1998; Multani et al., 1994; Scheibel and Scheibel, 1977; Swann et al., 2000), and the remaining synapses have included giant spines, tortuous spines, axon-free postsynaptic densities (PSDs), and synapses in aberrant locations (Baloyannis and Kim, 1979; Chen and Hillman, 1982; Fiala et al., 2002; Raisman and Field, 1973). Perisynaptic astroglial may also be an important component of the synaptic pathology of MTLE.

Previously, we demonstrated that three or more hours of recovery *in vitro* was required for rat hippocampal slices to recover from trauma after dissection and display excellent ultrastructure (Fiala et al., 2003). We applied these methods of recovery and rapid microwave-enhanced fixation (Jensen and Harris, 1989) to preserve synapses in slices from human hippocampus. Sections prepared for histological analysis revealed different patterns of mesial temporal sclerosis (MTS) of Type 1a or 1b (Blumcke et al., 2007). Three-dimensional reconstructions and unbiased volume analyses were obtained through serial section transmission electron microscopy

Mark R. Witcher is currently at Department of Neurosurgery, Wake Forest University, Winston-Salem, NC 27157, USA

Mark R. Lee is currently at Dell Children's Medical Center of Central Texas, Austin, TX 78723, USA

MRW, KMH, and SAK designed and performed the ssTEM experiments, completed the analyses, and wrote the article; YDP provided the clinical assessments; SS assessed the histology preparations; MRL performed the surgeries.

Grant sponsor: NIH; Grant numbers: T32 NRSA NS045543 (to MRW), NS21184, NS33574, and EB002170 (to KMH), NS057113 and NS062154 (to SAK); Grant Sponsors: American Academy of Neurology (to MRW), The Medical College of Georgia Intramural Grants Program (to SAK).

\*Correspondence to: Kristen M. Harris, PhD, Center for Learning and Memory, University of Texas at Austin, 1 University Station C7000, NMS 4.104, Austin, TX 78712-0805, USA. Email: kharris@mail.clm.utexas.edu or Sergei A. Kirov, PhD, Department of Neurosurgery, Medical College of Georgia, 1120 15th Street, CB-3706, Augusta, GA 30912, USA. E-mail: skirov@mcg.edu

Received 31 August 2009; Accepted 6 October 2009

DOI 10.1002/glia.20946

Published online 11 November 2009 in Wiley InterScience (www.interscience.wiley.com).

TABLE 1. Patients in This Study

Patient	Febrile Seizures	MRI findings	Duration (years)	Age at Surgery (years)	Follow-up (months)	Seizure Freedom	Gender	AEDs
A (control)	No	Signal change in temporal cortex	8	16	15	No	F	Levetiracetam, topiramate
B (mild)	No	Signal change in hippocampus	9.5	10	15	Yes	F	Oxcarbazepine, topiramate
C (moderate)	No	Signal change in hippocampus	4.5	17	12	Yes	F	Oxcarbazepine, topiramate, levetiracetam
D (severe)	Yes	Signal change in hippocampus	4	13	15	Yes	F	Oxcarbazepine, levetiracetam

Notes: Patient A had an extrahippocampal temporal mass lesion (ganglioglioma WHO-1) with a proliferative index less than 1% and developed a new seizure focus in frontal cortex after surgery, but never had hippocampal effects.

(ssTEM) to examine perisynaptic astroglial relationships and to understand whether there might be changes specifically associated with the synaptic and dendritic pathology of MTLE.

## MATERIALS AND METHODS

Patients were screened according to a series of clinical tests performed during routine presurgical assessment including clinical history, neurological tests, neuroimaging studies, neurodevelopment assessments, scalp electroencephalogram (EEG), and clinical pathologic examination. Results of all assessments were accessible from the patient's medical records for correlation with laboratory findings. Patients selected for study were all of female gender in their second decade of life (Table 1). All were treated with two or three antiepileptic drugs (AEDs) for at least 4 years without successful control of seizures. The AEDs included combinations of oxcarbazepine (Patients B, C, and D), topiramate (Patients A, B, and C), and/or levetiracetam (Patients A, C, and D). Patient A had an extrahippocampal temporal mass lesion (ganglioglioma WHO-1) with no hippocampal involvement and served as a histological control for assessing tissue from Patients B, C, and D as described below. Surgical anesthetic and en bloc hippocampectomy were similar between patients. Parent's informed consent documents and children's assent documents were obtained at the beginning of each study. All protocols were approved by the Institutional Review Board at the Medical College of Georgia.

### Quantitative Analysis of Histology

For Nissl staining, 5- $\mu$ m-thick sections were cut from paraffin blocks. Sections were air-dried overnight (37°C), deparaffinized in xylene (Fisher Scientific, Pittsburgh, PA), hydrated through graded alcohols to distilled water, and stained with 0.5% Cresyl ECHT Violet (Fisher Scientific) for 10 min. Sections were then rinsed in distilled water, dehydrated, cleared with xylene, and mounted on microscope slides for further examination.

For GFAP immunohistochemistry, 4- $\mu$ m-thick sections were cut from paraffin blocks and mounted on treated slides (Superfrost Plus, VWR Scientific Products, Suwanee, GA). Sections were air-dried overnight and then placed in a 60°C oven for 30 min. Sections were deparaffinized and processed through graded alcohols to distilled water. Endogenous peroxidase was quenched

with 0.3% H<sub>2</sub>O<sub>2</sub> in distilled water for 5 min followed by distilled water for 2 min and 1 $\times$  PBS for 5 min. Sections were then incubated with primary antibody GFAP (rabbit polyclonal) (Dako, Carpinteria, CA) at 1:4,000 dilution for 30 min at room temperature followed by two changes of 1 $\times$  PBS. Sections were then incubated with a Labelled Polymer conjugated to goat antimouse immunoglobulins (Envision plus HRP Kit, Dako) for 30 min and rinsed twice in 1 $\times$  PBS. Bound antibody was detected with DAB+ substrate kit (DAB+ substrate kit for peroxidase-HRP, Dako). Sections were then counterstained with hematoxylin (Thermo Fisher Scientific, Waltham, MA). Negative control sections went through the same protocol with the exception of the primary antibody.

Slides were scanned using the Aperio ScanScope CS digital slide scanner (Aperio, Vista, CA) with the Olympus 20 $\times$ /0.75 NA Plan Apo objective (Olympus America, Center Valley, PA) and additional 2.125 $\times$  magnification resulting in a lateral resolution of 0.22  $\mu$ m/pixel. Brightness and contrast adjustments were made for uniformity of appearance (Adobe Photoshop 7.0, Adobe Systems, San Jose, CA). Using the Aperio Spectrum<sup>TM</sup> digital pathology management software, we identified the best hippocampal section available for each sample (see Fig. 1). Serial sections were not available for these light microscopy analyses; hence, it was not possible to use modern stereological cell counting methods. Nevertheless, a systematic approach was used to count CA1 neurons and estimate their density in *stratum pyramidale* of proximal area CA1. Magnification was set at 20 $\times$  to obtain a total field size of 0.13 mm<sup>2</sup> in *s. pyramidale*. Six contiguous fields were captured across *s. pyramidale* beginning just distal to the junction with CA2 (Andrioli et al., 2007). All neuronal cell bodies completely contained within these viewing fields were counted and average densities were computed per case. The hippocampus from Patient A was used as a control for histological comparison among the cases (see Fig. 1). Tissue from Patient A had been collected prior to these studies and hence was not available for EM. Unfortunately, additional "normal" hippocampal controls did not become available during the 4.5 years of this study.

### Recovery of Human hippocampal Slices

Acute hippocampal slices were prepared immediately after resection according to standard methods (Kirov et al., 2004), because live recovery *in vitro* was needed to preserve ultrastructural integrity (Fiala et al., 2003;

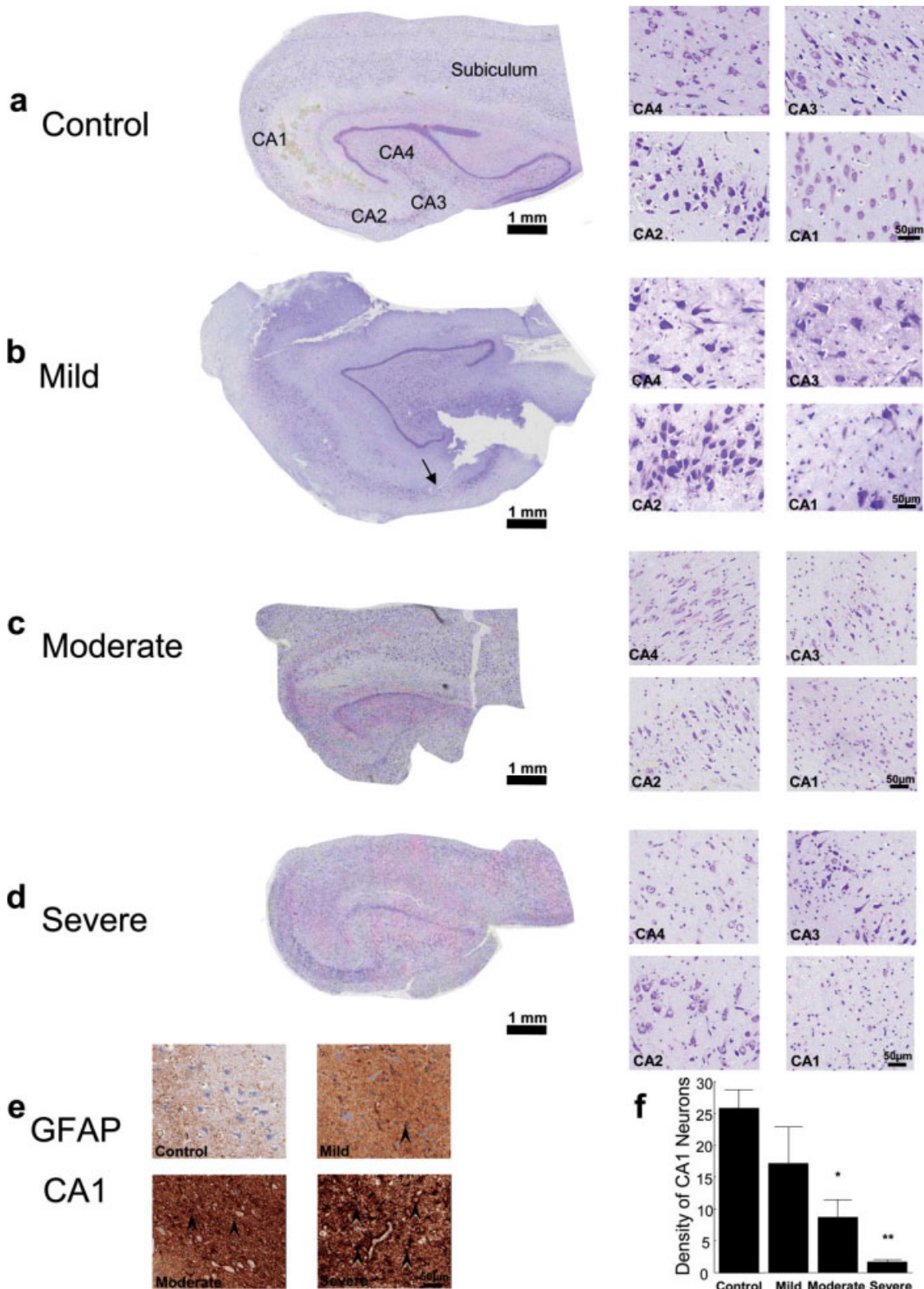


Fig. 1. Histology from human hippocampal surgical specimens. (a–d, left side) Nissl-stained transverse hippocampal sections (with proximal area CA1 indicated by an arrow in b, illustrated at the same scale). (a–d, right side) Subfields CA1–CA4 at higher magnification from each case. (e) Representative GFAP-labeled sections from CA1 *stratum pyramidale* in each case. Example hypertrophic reactive astroglia indicated by black arrowheads. (f) Quantification of Nissl-stained neurons in area CA1, where six sample areas of 130,000  $\mu\text{m}^2$  each were analyzed (mean  $\pm$  SEM, mild did not differ significantly from Control,  $P = 0.33$ ; moderate and severe differed significantly from Control,  $*P < 0.05$ ;  $**P < 0.0005$ ).

Kirov et al., 1999; Witcher et al., 2007). During surgery, it required less than 2 min to resect the hippocampus after cutting the main blood supply, resulting in healthy slices. A small sample of hippocampal tissue (~2 cm) was immediately cut and collected into ice-cold oxygenated sucrose-based ACSF (Sucrose-ACSF) containing 210 mM sucrose, 2.5 mM KCl, 25 mM NaHCO<sub>3</sub>, 1 mM NaH<sub>2</sub>PO<sub>4</sub>, 8 mM MgSO<sub>4</sub>, 10 mM glucose, pH 7.4, osmolality 290 mOsm/kg H<sub>2</sub>O, and transferred from the operating room to a laboratory adjacent to the operating suite. To protect against spine loss (Kirov et al., 2004), acute hippocampal slices (400 μm) were prepared with ice-cold Sucrose-ACSF using a vibrating-blade microtome (VT1000S, Leica Instruments). Slices were transferred by a wide-bore pipette into an incubation chamber and placed onto 0.4-μm millicell inserts (Millipore, Bedford, MA) positioned over wells containing standard ACSF and maintained at the interface of humidified 95% O<sub>2</sub>–5% CO<sub>2</sub> atmosphere at 32°C, pH 7.4. The standard ACSF contained 120 mM NaCl, 2.5 mM KCl, 25 mM NaHCO<sub>3</sub>, 1 mM NaH<sub>2</sub>PO<sub>4</sub>, 2.5 mM CaCl<sub>2</sub>, 1.3 mM MgSO<sub>4</sub>, 10 mM glucose, pH 7.4, resulting in 290 mOsm/kg H<sub>2</sub>O.

The average delay between surgical resection and placing the first slice into the incubation chamber was about 5 min. Slices were incubated for 3–4 h for ultrastructural recovery (Fiala et al., 2003) and then rapidly fixed during 8 s of microwave irradiation in mixed aldehydes (2% paraformaldehyde, 6% glutaraldehyde in 0.1 M cacodylate buffer, pH 7.4, and containing 2 mM CaCl<sub>2</sub> and 4 mM MgCl<sub>2</sub>) and stored overnight in fixative at room temperature (Jensen and Harris, 1989).

### Electron Microscopy

A small piece of tissue containing the CA1 region was microdissected and subsequently processed through reduced osmium [1% OsO<sub>4</sub> with 1.5% K<sub>4</sub>Fe(CN)<sub>6</sub>] followed by 1% OsO<sub>4</sub>, to preserve and enhance membranes, and then exposed to 1% uranyl acetate, dehydrated, and embedded in Epoxy Resins and hardened for 48 h at 60°C (Harris et al., 2006). Samples from the middle of *s. radiatum* at an optimal depth of ~150–200 μm beneath the slice surface were obtained from each of Patients B, C, and D for ssTEM. Series of 40–50 sections, each ~45 nm thick, were cut on an Ultracut T ultramicrotome (Leica Instruments). A total of nine series, three from each case, were collected on Pioloform-coated slot grids (Synaptek, Electron Microscopy Sciences) and stained with ethanolic uranyl acetate followed by Reynolds' lead citrate (Harris et al., 2006). These series were positioned to be separated by more than 100 μm to avoid overlapping astrocytic processes (Bushong et al., 2002, 2004). These protocols produced well-stained and readily identifiable neuronal and astroglial processes (Fig. 2a–c).

### Quantification Through ssTEM

Serial sections were photographed at the JEOL 1230 transmission electron microscope (Peabody, MA). Images

were digitally captured at a magnification of 5,000× using the GATAN UltraScan 4000 camera (Gatan, Pleasanton, CA). Series were coded and analyzed blind to patient (Fig. 2d). Images were digitally optimized for brightness and contrast to visualize structures of interest. Some images in the figures are colorized to highlight particular structures. Three-dimensional alignment, reconstruction, and analyses were performed using the RECONSTRUCT™ software (Fiala, 2005), which is freely available (<http://synapses.clm.utexas.edu/tools/index.stm>). Pixel size was calibrated relative to a diffraction grating replica (Ernest F. Fullam, Latham, NY), and section thickness was calibrated using the cylindrical diameters method (Fiala and Harris, 2001a). Surface areas of cross-sectioned synapses were computed by measuring their lengths on individual sections, multiplying by section thickness and summing over sections. Synapses cut enface were outlined and the enclosed area calculated. Surfaced reconstructions were completed using RECONSTRUCT™ for most of the figures and OsiriX software for Fig. 6d (Rosset et al., 2004).

### Dendritic Spine Classifications

Dendritic spines were classified as thin, mushroom, stubby, and giant (Fiala et al., 2002; Harris et al., 1992). Briefly, spines were judged *thin* if ssTEM revealed the length to be greater than the neck diameter, and the diameter of the neck and head to be similar. Spines were classified as *mushroom* if the diameter of the head was greater than 0.6 μm and was much greater than the diameter of the neck. *Stubby* spines had the diameter of the neck similar to the total length of the spine. *Giant* spines had large heads and a reconstructed volume bigger than most mushroom spines and multiple small synapses with different presynaptic axons.

### Presynaptic Vesicle Quantification

We attempted to quantify all presynaptic vesicles. Presynaptic vesicle membranes were less distinct in tissue from Patient D and somewhat less distinct in the tissue from Patient C, relative to the tissue from Patient B. Hence, the total number of presynaptic vesicles could not be reliably counted. Fortunately, it was possible to quantify the number of docked presynaptic vesicles. Docked presynaptic vesicles were identified through serial sections and were counted if their membrane was adjacent to the plasma membrane of the presynaptic axon at the active zones defined by the extent of the postsynaptic density [see also Harris and Sultan (1995), Henze et al. (2002), and Xu-Friedman et al. (2001)].

### Statistics

Excel software (Microsoft, Redwood, CA) was used to organize the data, and Statistica (StatSoft, Tulsa,

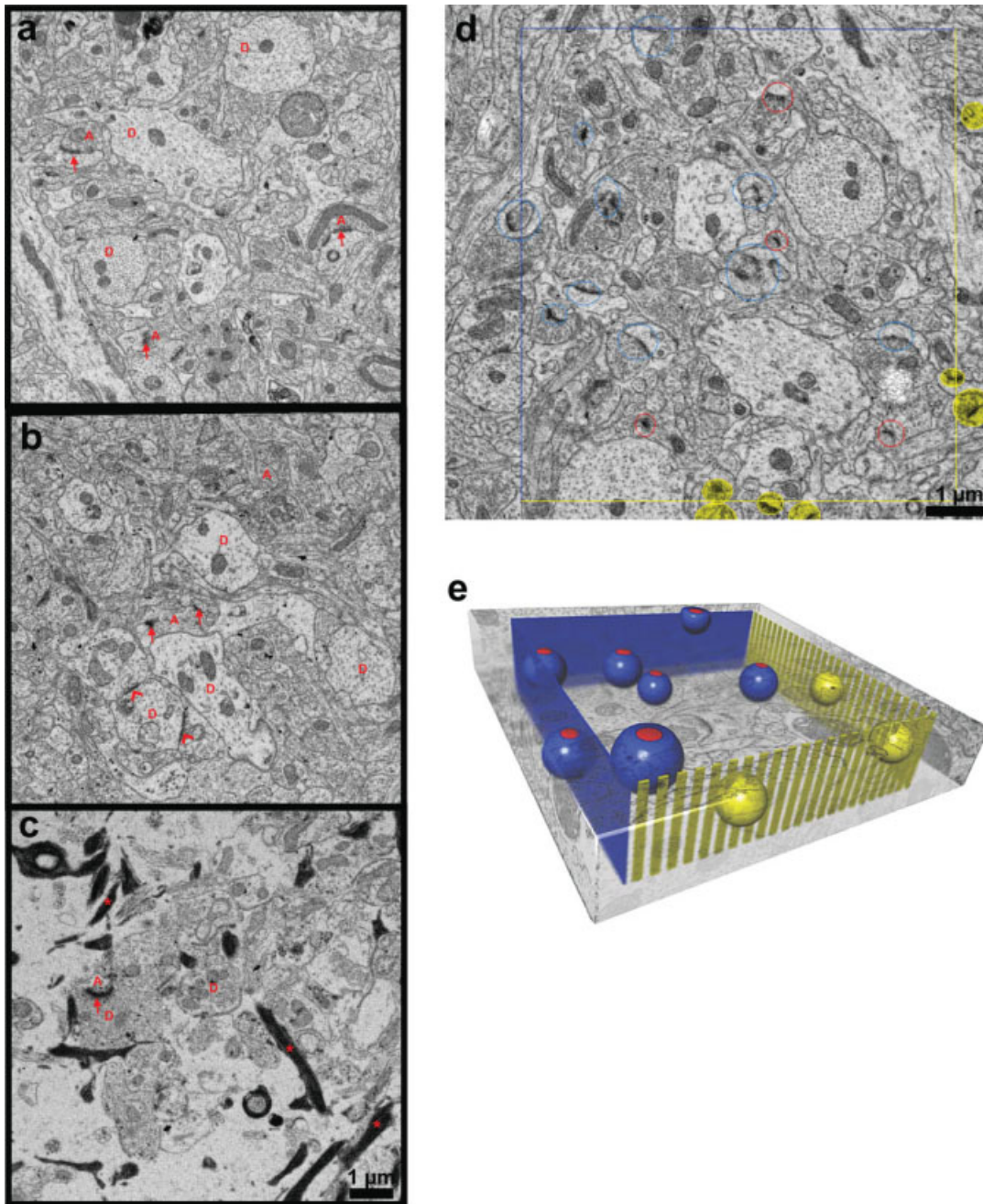


Fig. 2. Ultrastructural images from each case and illustration of the unbiased method. Mild (a) and moderate (b) cases with compact neuropil and little extracellular space had dendrites [D] with intact cytoplasm, organelles, and well-ordered arrays of microtubules. Asymmetric (red arrows) and symmetric (red chevrons) synapses apposed to axonal boutons [red A]. (c) Severe case had neuropil with more extracellular space, fewer dendrites [D], axons [A], synapses (arrows), and astroglial processes filled with densely stained filaments (stars). Unbiased stereological analysis: (d) Central section of series from mild case, and (e) schematic of the unbiased analysis. Synapses counted if their PSDs

were completely contained within sampling volume or intersected inclusion faces (blue lines in d, blue planes in e). Synapses excluded if they intersected exclusion faces (yellow lines d, yellow "picket fence" in e). Synapses intersecting bottom face were included and synapses intersecting top face were excluded (top and bottom faces not shown). Included synapses were encircled with red on the first section where the PSD appeared in the series and then circled with dark blue on adjacent serial sections to identify them and assure that none were double counted. Red and dark blue spheres illustrate included synapses and yellow spheres illustrate excluded synapses in e.

OK) was used to obtain means and standard deviations and to perform regression analyses, ANOVAs, ANCOVAs, and post-hoc *t*-tests. Data from the three series in each patient were grouped by patient where appropriate and graphed as mean  $\pm$  SEM. Criterion *P* was  $<0.05$ .

GLIA

## RESULTS

### Relative Differences in the Histology of Hippocampal Tissue Selected for ssTEM

Histological assessment of hippocampal sclerosis was based on light microscopic evaluation of formalin-fixed,

paraffin-embedded, Nissl-stained, and GFAP immunostained sections. Hippocampal tissue from Patient A provided a “control” comparison without detectable histopathologies (Fig. 1a and Table 1). Patient B had mesial temporal sclerosis (MTS) Type 1a (Blumcke et al., 2007) with less than 50% neuronal loss in the hippocampal CA1 and slight involvement of CA3 and CA4 regions (Fig. 1b,f). Mild to moderate reactive astrogliosis was most prominent in the proximal CA1, where it was tile-like and focally interdigitating (Fig. 1e). Hence, for the purpose of quantitative analysis with ssTEM, the hippocampus from Patient B was considered to have a “mild pathology.” Patient C also had classical MTS Type 1a and demonstrated more than 50% neuronal loss in CA1 with substantial involvement of CA3 and CA4 subfields (Fig. 1c,f) and moderate reactive astrogliosis in the CA1 region (Fig. 1e) and therefore was considered to have a “moderate pathology.” Patient D had severe MTS Type 1b with more than 90% neuronal loss with hypertrophic reactive astrogliosis in the CA1 region (Fig. 1d–f) and more than 50% neuronal loss and astrogliosis affecting the CA3 and CA4 regions. Thus, Patient D was considered to have a “severe pathology.” The CA2 and subicular subfields as well as the parahippocampal gyri were preserved within normal histologic limits in all three cases. Patient A was initially seizure-free, but subsequently developed a focus in the frontal lobe. Patients B, C, and D were seizure-free at a follow-up period of at least 12 months after surgery.

### Ultrastructural Disorganization Accompanied Progressive Histological Changes

Dendrites in the mild case had intact membranes, uniformly spaced microtubules, clear cytoplasm, and intact subcellular organelles (Fig. 2a). Asymmetric synapses were evident on dendritic spines and their presynaptic axonal boutons contained round synaptic vesicles typical of excitatory glutamatergic synapses (Fig. 2a). Symmetric synapses typical of inhibitory GABAergic synapses were evident along some dendritic shafts. Presynaptic membranes were slightly less distinct in the moderate case (Fig. 2b), while other features were similar to the mild case. In contrast, dendrites in the severe case had intact membranes with subcellular organelles and clear cytoplasm, but microtubules arrays were disorganized, synapses were rare, and presynaptic membranes were much less distinct as compared with the mild case. The mild and moderate cases had compact neuropil with little extracellular space (Fig. 2a,b), whereas there was much more extracellular space and numerous astroglial processes were filled with dense-staining filaments in the severe case (Fig. 2c). Thus, progressive ultrastructural disorganization paralleled progressive histological changes.

### Unbiased Analysis of Spines and Synapses in Volumes of Human Hippocampal Neuropil

We used ssTEM and unbiased volumetric analysis (Fiala and Harris, 2001b) to quantify ultrastructural

relationships in the neuropil (Fig. 2d,e). This analysis expands beyond traditional two-section disector stereology (West et al., 1988), because it allows for more complete identifications and measurements of objects including dendrites, synapses, spines, axons, and perisynaptic astroglia (Fig. 2a,b). Three samples  $\sim 100 \mu\text{m}^3$  each were photographed from each hippocampal slice providing  $\sim 300 \mu\text{m}^3$  per patient and  $900 \mu\text{m}^3$  in total. Overall, 329 synapses were characterized in 3D from these samples with 191 synapses in the mild, 113 in the moderate, and 25 in the severe cases.

### Progressive Synapse Loss

Asymmetric, presumably excitatory, synapses were characterized by a thickened postsynaptic density (PSD) adjacent to a presynaptic axonal bouton containing round clear vesicles (Fig. 3a–e). Symmetric, presumably inhibitory or modulatory, synapses occurred directly on the dendritic shafts and were characterized by uniformly thin pre- and postsynaptic densities and smaller, pleomorphic vesicles in the presynaptic axonal bouton (Fig. 3f). Mild and moderate pathologies had normal-appearing spines with a single macular PSD located on thin shaped spines (Fig. 3g,h) and macular, perforated, or segmented PSDs located on mushroom-shaped spines (Fig. 3i,j).

The density of asymmetric synapses was significantly less in the moderate and severe cases than in the mild case (Fig. 3k). Symmetric synapses are normally rare in *s. radiatum* of area CA1; however, their density was slightly elevated in moderate relative to mild case, but none were observed in the severe case (Fig. 3k). Similarly, the ratio of symmetric to asymmetric synapses was 4% in mild and 12% in moderate tissue. Spines with a thin shape accounted for  $\sim 84\%$  of all asymmetric spine synapses in the mild case, whereas a significant decrease in the frequency of mushroom spines resulted in a relative increase in thin spines in the moderate case (Fig. 3l). There were also significantly more stubby spines ( $\sim 6\%$ ) in the moderate than the mild ( $\sim 1\%$ ) case. Only one thin and no mushroom or stubby spines were found in the severe case (Fig. 3l).

### Multisynaptic “Giant” Dendritic Spines

In the severe case, most (96%) of the 24 synapses were located on seven multisynaptic “giant” spines (see Fig. 4). These spines had large heads with multiple postsynaptic densities (PSDs) that formed synapses with different presynaptic axonal boutons (Fig. 4a–c). The reconstructed volume of the giant spine presented in Fig. 4b is  $\sim 0.44 \mu\text{m}^3$ . For comparison, the reconstructed volumes of thin spines presented in Fig. 3g and Fig. 3h were  $\sim 0.048 \mu\text{m}^3$  and  $\sim 0.12 \mu\text{m}^3$ , respectively, while the reconstructed volumes of mushroom spines were  $\sim 0.38 \mu\text{m}^3$  (Fig. 3i) and  $\sim 0.35 \mu\text{m}^3$  (Fig. 3j). Multisynaptic spines were rare in the mild and moderate cases (7 and

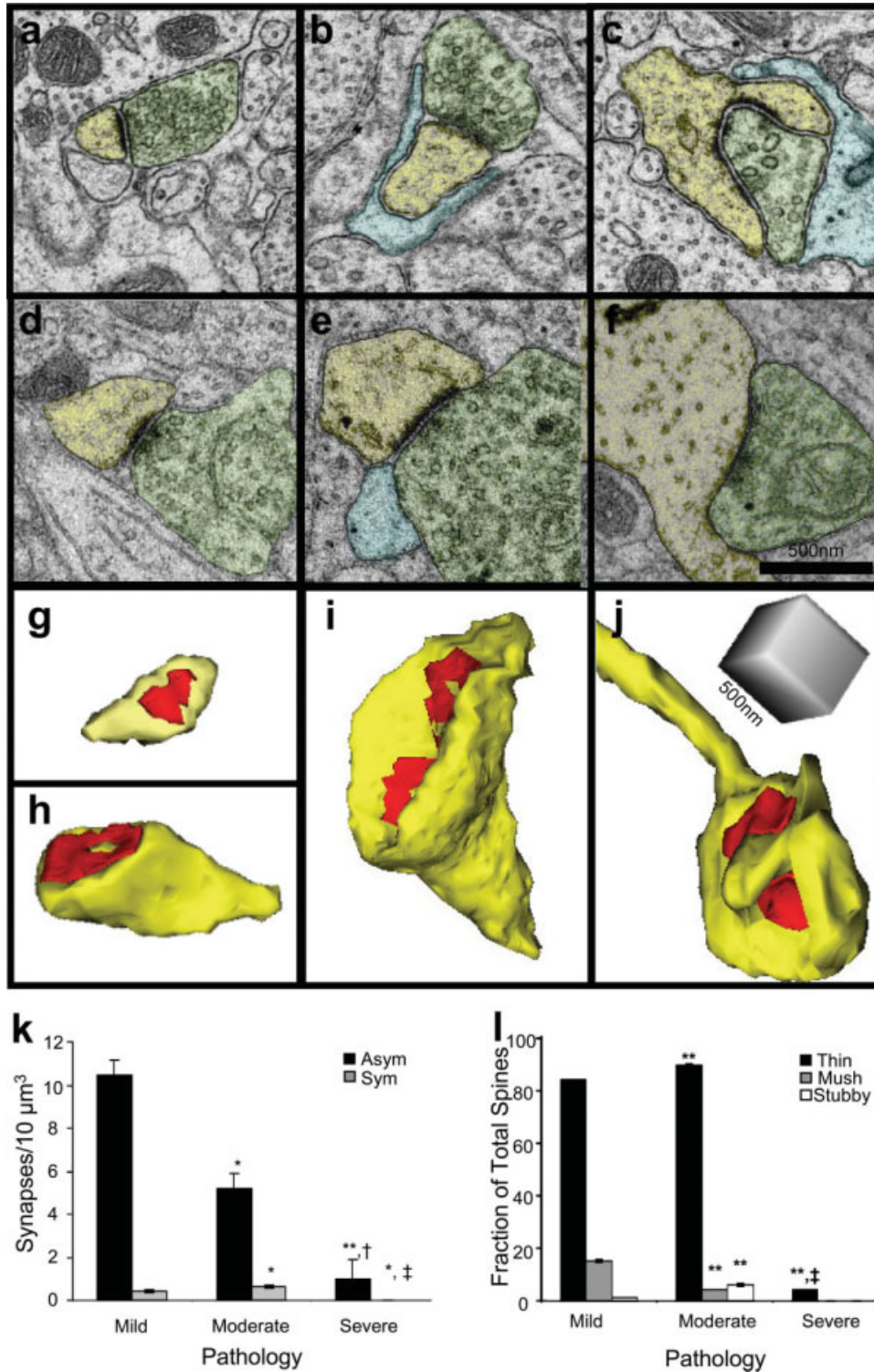


Fig. 3. Spine synapses in human hippocampus. In the mild case, (a) typical thin spine (yellow) and (b) typical thin and (c) mushroom spines with perisynaptic astroglia (light blue) form synapses with axonal boutons containing round clear vesicles (green). Typical (d) thin and (e) mushroom spines in the moderate case. (f) Symmetric synapse on a dendritic shaft in the moderate case (scale bar in f is for a–f). Reconstructions of thin spines in the mild (g) and moderate (h) cases, and

mushroom spines in the mild (i) and moderate (j) cases (scale cube in j is for g–j). (k) Volumetric densities of asymmetric synapses (black bars) and symmetric synapses (gray bars) in each case ( $*P < 0.05$ ;  $**P < 0.0005$  relative to mild;  $^\dagger P < 0.05$ ;  $^\ddagger P < 0.0005$  relative to moderate). (l) Fraction of spines in the thin (black), mushroom (gray), and stubby (white) shape categories ( $**P < 0.0001$  relative to mild,  $^\ddagger P < 0.0001$  relative to moderate).

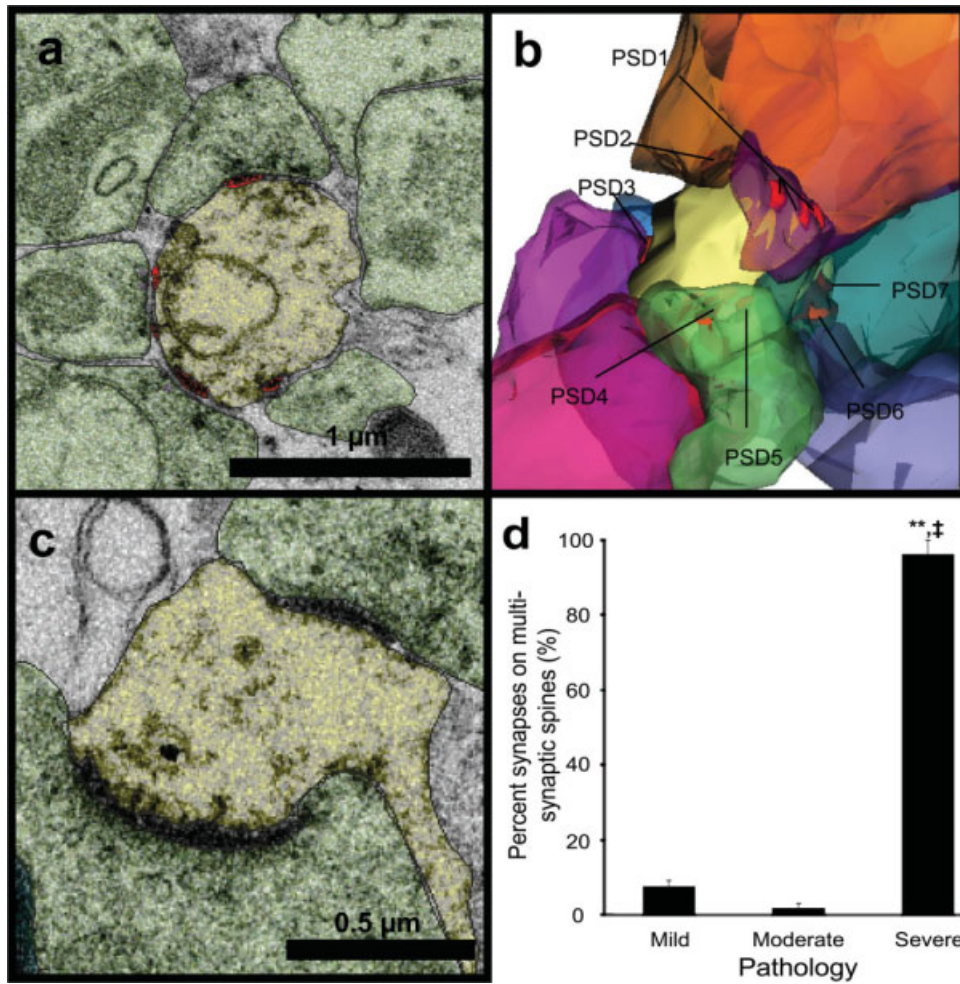


Fig. 4. Multisynaptic spines in the severe case. (a) Electron micrograph of multisynaptic giant spine (yellow) with four synapses (red) and seven axons that eventually synapse with this spine visible on this one section. (b) 3D reconstruction of the same multisynaptic giant spine showing all nine of its presynaptic axonal boutons (multicolored) and seven of its PSDs (eight and nine are hidden). (c) A smaller multisynaptic spine that had three synapses with different presynaptic axons, two are on this section and one is on another section. (d) Multisynaptic spines were rare in the mild and moderate conditions, whereas nearly all of the synapses remaining in the severe condition were on multisynaptic giant spines (\*\* $P < 0.0001$  relative to mild, † $P < 0.0001$  relative to moderate).

2%, respectively; Fig. 4d), and in these conditions, they were similar in shape and size to the thin and mushroom spines.

#### Number of Presynaptic Docked Vesicles Was Proportional to Synapse Area

We have previously shown that the number of docked vesicles correlates well with the total number of vesicles in a presynaptic bouton and with the size of the PSD in the rat hippocampus (Harris and Sultan, 1995; Lisman and Harris, 1993). Here, we measured the surface area of PSDs and quantified docked vesicles adjacent to PSDs in the mild, moderate, and severe cases (Fig. 5a–g). The number of docked vesicles well-correlated with the size of the PSD in the mild and moderate cases (Fig. 5h). The range in size of individual PSDs on the multisynaptic spines was  $0.009\text{--}0.275 \mu\text{m}^2$  with a mean value of

$0.065 \pm 0.055 \mu\text{m}^2$ , which was significantly larger than those on typical thin spines with a mean value of  $0.041 \pm 0.026 \mu\text{m}^2$  ( $P < 0.05$ ), but smaller than typical mushroom spines with their mean value of  $0.161 \pm 0.099 \mu\text{m}^2$  ( $P < 0.0001$ ). Too few synapses remained to determine whether this trend also held for the severe case. These findings suggest that the correlation between presynaptic vesicle numbers and PSD surface area also holds in human hippocampus, but might be disrupted in severe case.

#### Astrogliosis and Specialized Interastroglial Junctions

At the ultrastructural level, normal astroglial processes were identified by their interdigitation among neuronal processes, the presence of glycogen granules in a clear cytoplasm, and the restriction of bundles of inter-

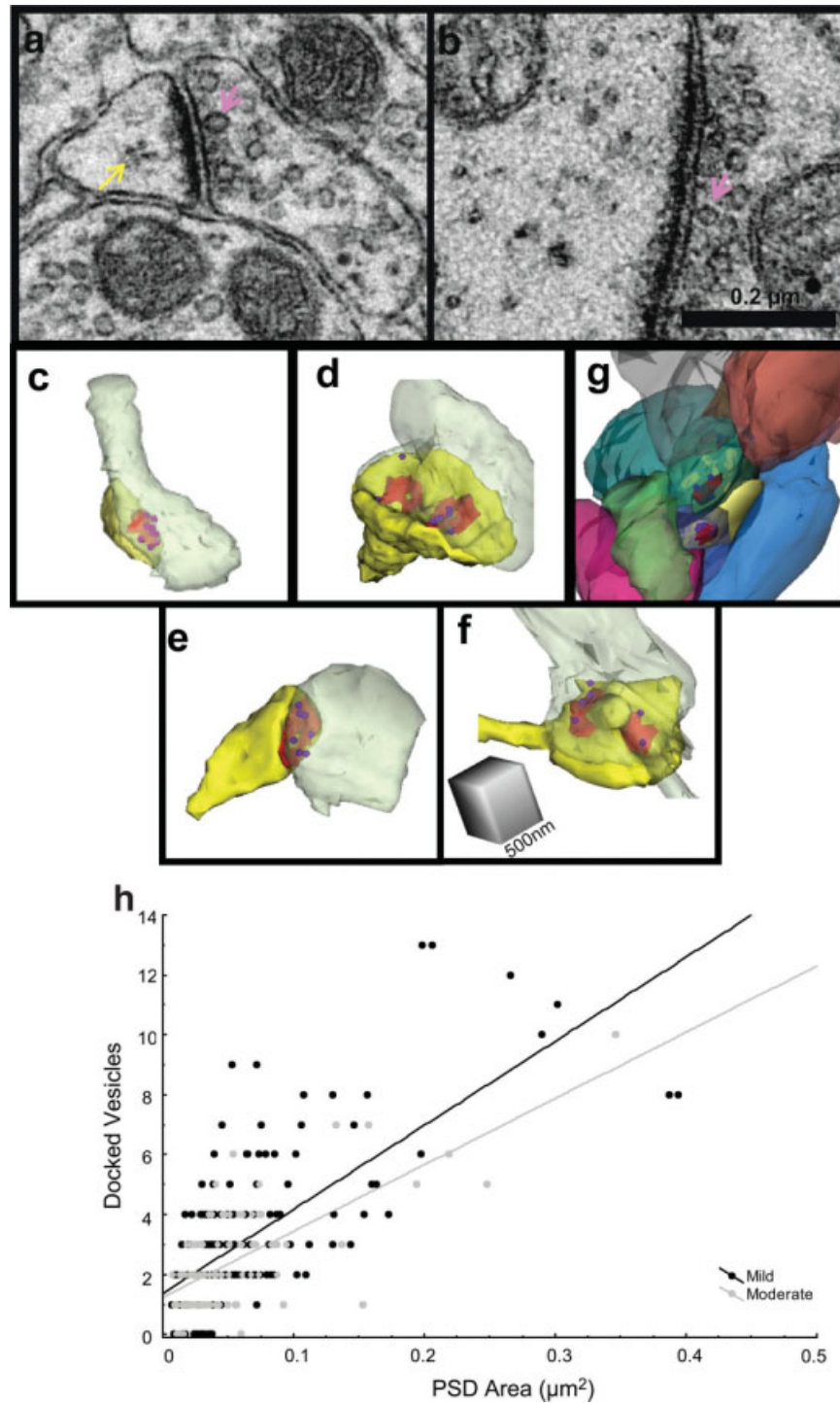


Fig. 5. Larger synapses had more docked presynaptic vesicles. (a) Docked vesicle (purple arrow) in the presynaptic bouton associated with a thin spine from the mild case. Also noted, though not quantified, is a polyribosome in the spine head (yellow arrow). (b) Docked vesicle (purple arrow) at a shaft synapse in the mild case (scale bar is for a and b). 3D reconstructions show docked vesicles (purple) at (c) thin and

(d) mushroom spines in the mild case and (e) thin and (f) mushroom spines in the moderate case, and (g) a multisynaptic spine in the severe case (scale cube in f is for c–g). (h) Docked vesicle number correlated with PSD area in the mild ( $r = 0.69$ ,  $P < 0.0001$ ) and moderate ( $r = 0.68$ ,  $P < 0.0001$ ) cases.

mediate filaments to cell soma and large proximal processes (Bushong et al., 2002; Ventura and Harris, 1999). The mild case had normal-appearing astroglial processes (Fig. 6a). In the moderate case, some of the thin astro-

glial processes had bundles of filaments along their lengths (Fig. 6b), whereas thin astroglial processes (0.20–0.35 µm in diameter) in the severe case were filled with dense staining filaments obscuring the cytoplasm

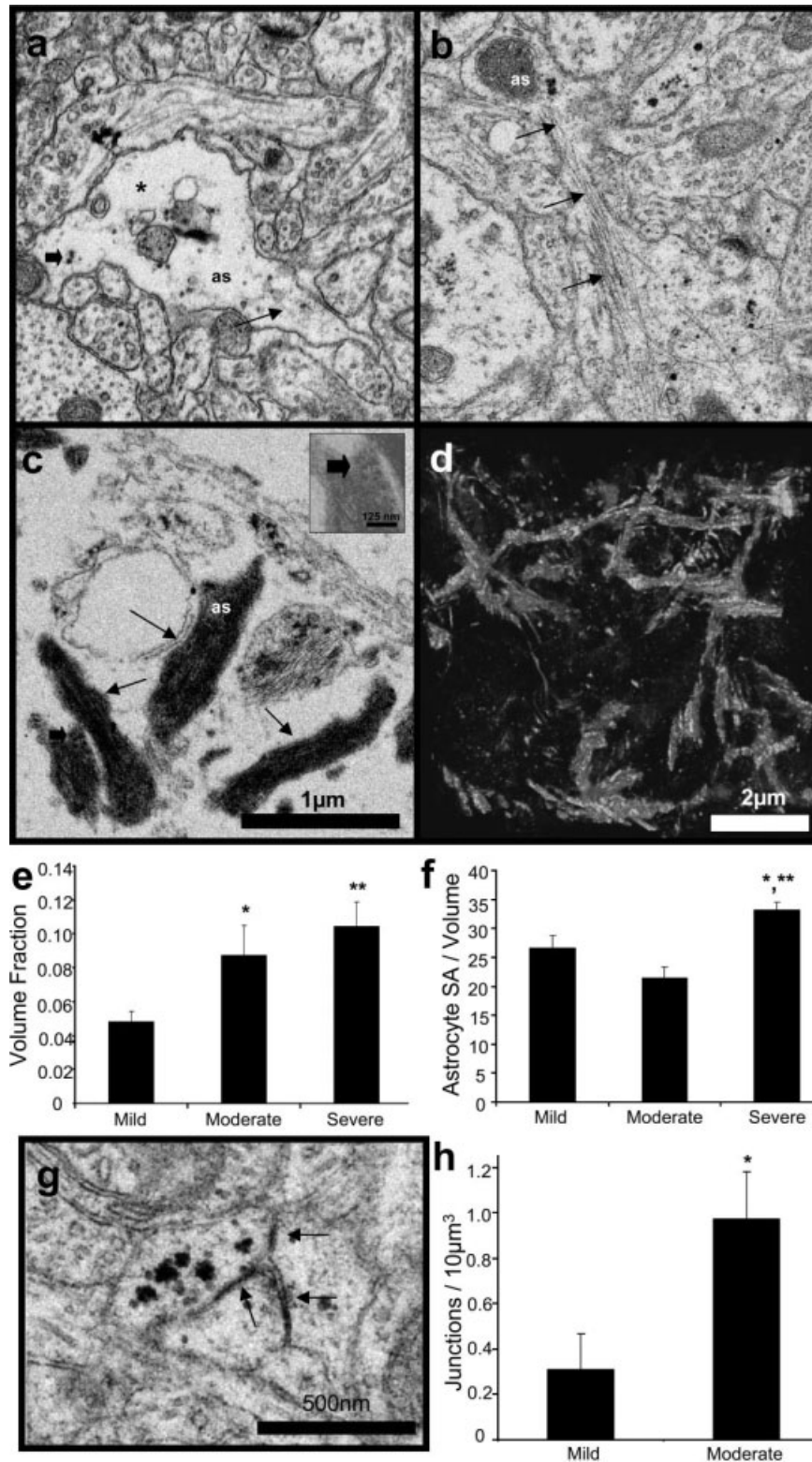


Fig. 6. Astroglial morphology. (a) Large astroglial process (as) from the mild case illustrates the relatively “normal” appearance with clear cytoplasm (\*), glycogen granules (thick arrow), and no or few filaments (thin arrow) in small processes. (b) Numerous filaments (arrows) nearly fill a relatively thin astroglial process (as) in the moderate case. (c) Astroglial processes (as, arrows) in the severe case were filled with filaments, so much so that their cytoplasm was nearly obscured. By adjusting the contrast, glycogen granules became apparent in some portions of the processes (thick arrow, and inset). Scale bar in (c) is for (a–c). (d)

Three-dimensional reconstruction of the dense astroglial processes (negative, white) from the severe case illustrating their arrangement in the tissue. (e) Relative to the mild case, the fraction of the total sample volume occupied by astroglial processes was greater in the moderate (\* $P < 0.05$ ) and severe (\*\* $P < 0.005$ ) cases. (f) The astrocytic surface area/volume ratio was greater in the severe than the mild (\* $P < 0.05$ ) or moderate (\*\* $P < 0.001$ ) cases. (g) Example junctions (arrows) between apposed astrocytic processes from moderate case. (h) More astrocytic junctions were present in moderate than mild case (\* $P < 0.05$ ).

(Fig. 6c). Reducing image contrast revealed glycogen granules in some of the astroglial processes in the severe case (Fig. 6c, inset). Three-dimensional reconstruction of these dense staining processes showed a complex heterogeneous arrangement within the neuropil, which was particularly obvious when displayed in reverse color (Fig. 6d). The volume fraction of astroglial processes was greater in the moderate ( $8.7 \pm 2\%$ ) compared with the mild case ( $4.8 \pm 0.6\%$ , Fig. 6e), and the dark astroglial processes occupied  $10.4 \pm 1\%$  of the sample volumes in the severe case. The ratio of surface area to volume of astroglial processes did not differ between the mild or moderate cases (Fig. 6f), but was greater along the thin densely stained processes in the severe condition.

Junctional specializations were observed between astroglial processes (Fig. 6g). Three-dimensional quantification showed a significantly lower frequency of these astroglial junctions in the mild ( $0.31/10 \mu\text{m}^3$ ) than the moderate ( $0.97/10 \mu\text{m}^3$ ) case (Fig. 6h). The dark aggregates of filaments in astroglial processes in the severe case obscured membranes; hence, it was not possible to ascertain whether these junctions were present in this condition.

### Relationships Between Perisynaptic Astroglia and Human Hippocampal Synapses

The axon–spine interface (ASI) was examined through serial sections to determine the locations of perisynaptic astroglia in the mild (Figs. 3b,c and 7a), moderate (Figs. 3e and 7b), and severe (Figs. 4a,c and 7c) cases. In the mild and moderate cases, 40 and 46% of synapses had astroglial processes present in the ASI, while in the severe case only 16% of the multisynaptic giant spines had perisynaptic astroglia (Fig. 7d). In all three cases, synapses with perisynaptic astroglia were larger than synapses without (Fig. 7e). Only 1% of the synapses were completely surrounded by perisynaptic astroglia; hence, at 99% of all synapses, at least part of the ASI perimeter had no perisynaptic astroglia, leaving open a route for spillover of glutamate and other substances. The length of this open perimeter, i.e. astroglia-free length, was computed in 3D for each synapse (Witcher et al., 2007). There was a strong positive correlation between the astroglia-free length of the ASI perimeter and PSD area at synapses in the mild and moderate cases (Fig. 7f). Thus, larger synapses also had more access to substances in the extracellular space.

The shortest astroglia-free route was measured from the edge of the ASI through extracellular space to the nearest neighboring synapse either within or across serial sections as previously described (Witcher et al., 2007). These distances were measured in a subset of 73 synapses that was selected at equal intervals across the full range of PSD sizes in all three cases. Most synapses had neighbors located within  $1.5 \mu\text{m}$ , and the greatest distance measured along an astroglia-free path through the extracellular space (ECS) was  $3.3 \mu\text{m}$ . These distances

did not correlate with synapse size, degree of pathology, or the presence/absence of perisynaptic astroglia at the ASI. Interestingly, although there was a greater occupancy of glia in the neuropil of the moderate case, the remaining synapses were separated by longer astroglia-free distances than synapses in the mild case, suggesting that the astroglial processes do not simply hypertrophy around and between the remaining synapses (Fig. 7g). Since there were so few synapses left in the severe case, it was not possible to determine average astroglia-free path lengths between giant spines. Instead, neighboring synapses on a single giant spine head were nearly contiguous with one another with no interdigitating astroglial processes (Fig. 7c).

## DISCUSSION

Hippocampal slices prepared immediately after surgical resections were maintained *in vitro* for high-quality ultrastructural recovery and preservation. Perisynaptic astroglial processes were preferentially associated with larger synapses in the human hippocampus, like the adult rat model system (Witcher et al., 2007). The perimeters of the axon–spine interfaces were only partially surrounded by astroglial processes so that all these human synapses had some access to substances in the extracellular space, like the adult rat hippocampus. Progressive dendritic and axonal disruption, synapse loss, and astrogliosis were associated with increasing severity of the MTLE histopathology. In addition, specialized interastroglial junctions were greater in the moderate than the mild case suggesting that signaling between astrocytes might also increase with severity of MTLE histopathology.

### Variation Among Patients

The presurgery duration of the seizure disorder was opposite to the histopathological findings, with mild being longer than moderate, which was longer than severe. Differences in age bracketed the histopathology with moderate being oldest. According to pathological classification for MTS (Blumcke et al., 2007), Patients B and C had MTS Type 1a, while Patient D had MTS Type 1b with severe histopathology. We further distinguished patterns of histopathology in Patients B and C through quantification of neuron loss and astrogliosis in light microscopy as mild and moderate. To control for the possible influences of AEDs, we selected patients with overlapping medication profiles. The youngest patients did not have menstruation; however, previous studies from ovariectomized rats and nonhuman primates showed only a 20–30% phasic fluctuation in synapse number under the influence of gonadal hormones (Leranth et al., 2002; Woolley and McEwen, 1992; Woolley et al., 1996). Synapse density was  $\sim 50$  and 90% less in the moderate and severe, relative to the mild case. Thus, differences in duration of epilepsy, age of the

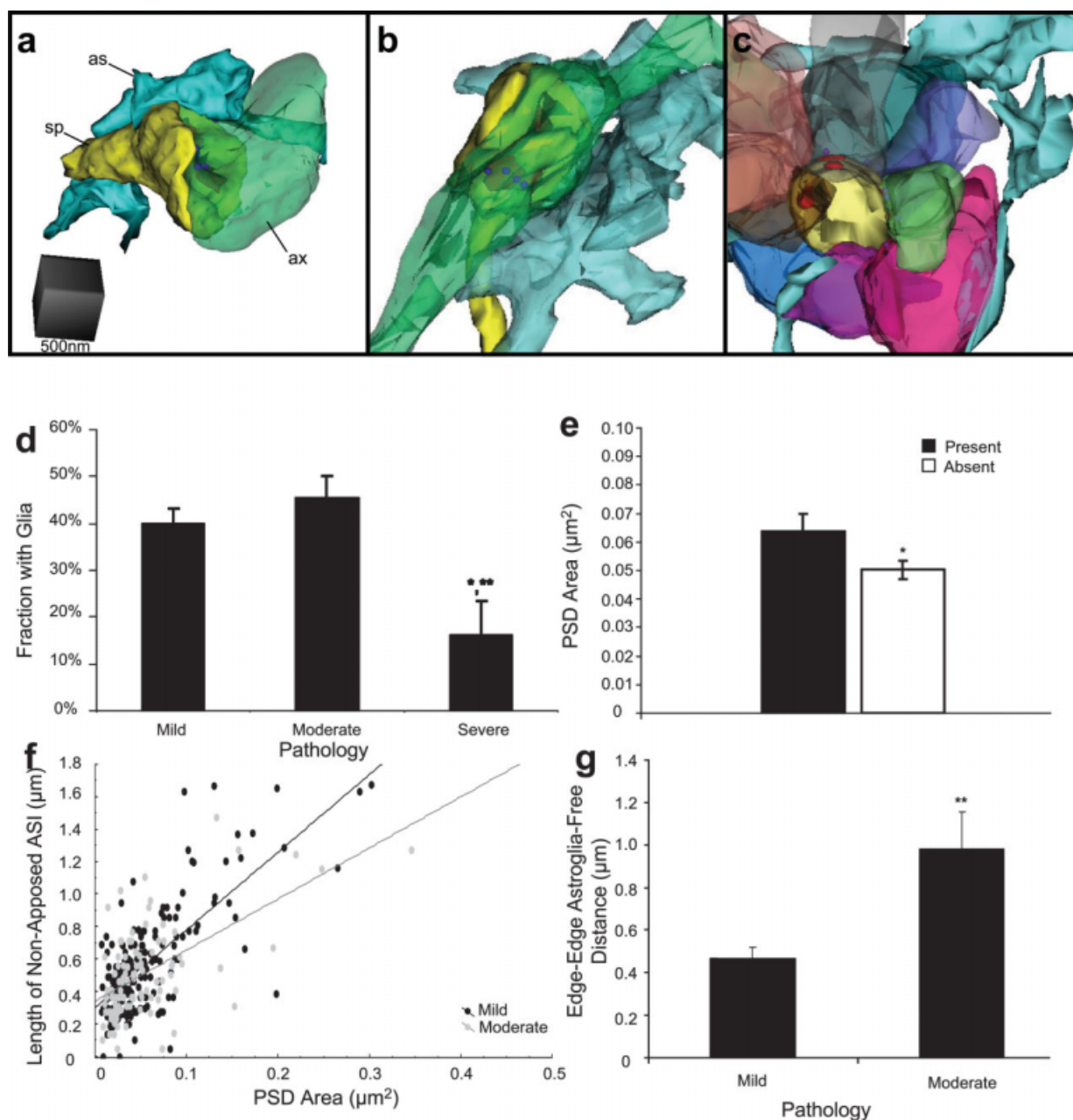


Fig. 7. Perisynaptic astroglia. 3D reconstructions from the mild (a) and moderate (b) cases show perisynaptic astroglial processes (turquoise) at the edges of synapses (PSDs, red) between dendritic spines (yellow) and presynaptic axons (green). (c) In the severe case, the astroglial processes (turquoise) hovered around the periphery of many presynaptic axons (multicolored), which synapses on a single multisynaptic spine (yellow). (d) Fraction of synapses with perisynaptic astroglia at the ASI is less in the severe than mild ( $*P < 0.05$ ) or moderate ( $**P <$

0.01) cases. (e) Synapses were smaller when astroglial processes were absent from the ASI ( $*P < 0.05$ ). (f) Correlation between total PSD area and the length of the ASI perimeter not apposed by astroglial processes (mild,  $r = 0.73$ ,  $P < 0.0001$ ; moderate,  $r = 0.58$ ,  $P < 0.0001$ ; severe,  $r = 0.28$ ,  $P = 0.18$ , data not shown). (g) The average astroglia-free distance through extracellular space to the nearest neighboring synapse was greater in moderate ( $0.98 \pm 0.17 \mu\text{m}$ ) than the mild ( $0.46 \pm 0.05 \mu\text{m}$ ) case ( $**P < 0.01$ ).

patient, AED, or phases of the menstrual cycle were not likely to be responsible for the reported findings.

### Human Hippocampal Synapses and Dendritic Spines

Dendritic spines in the mild and moderate cases had normal thin and mushroom shapes with dimensions

comparable to those found in normal adult rat hippocampus (Harris and Stevens, 1989). Synapse size well-correlated with the number of docked presynaptic vesicles suggesting coordination between pre- and postsynaptic composition and dimensions occurs in the human hippocampus like in the rat hippocampus (Harris and Stevens, 1989; Harris and Sultan, 1995; Lisman and Harris, 1994). Epileptic seizures have long

been associated with dendritic spine loss (Jiang et al., 1998; Multani et al., 1994; Scheibel and Scheibel, 1977; Swann et al., 2000), which has been attributed to calcium- and glutamate-mediated excitotoxicity (Swann et al., 2000). Spine loss can also result from partial deafferentation or activity-dependent pruning (Fiala et al., 2002; Jiang et al., 1998; Parnavelas et al., 1974; Paul and Scheibel, 1986; Swann et al., 2000). In the severe case, a few multisynaptic spines remained and have been referred to as “giant spines” (Fiala et al., 2002). Their measured volumes were only ~15% larger than mushroom spines and the size of the individual PSDs on multisynaptic spines was smaller than average mushroom PSDs. Thus, the multisynaptic spines appear to have resulted from competition among axons for synaptic sites on the few spines that were present in the severe case. Together these findings suggest that multisynaptic or “giant” spines were unlikely to be the original cause of the epileptic pathophysiology.

The ratio of symmetric (inhibitory) to asymmetric (excitatory) synapses in the mild case was low and similar to that found in normal adult rat hippocampus (Megias et al., 2001). More inhibitory input in the moderate case could indicate reactive inhibitory synaptogenesis, while absence of symmetric synapses in the severe case might signify reduced inhibition. The significance of this finding is not clear, because diverse modifications of inhibitory circuits in epileptic human hippocampus are often not correlated with specific histopathological alterations (Arellano et al., 2004).

### Effects of Astroglial Processes and Elevation in Specialized Interastroglial Junctions

We also found more astroglial processes with increasing histopathology and an elevation in intermediate filaments to the point where they obscured the cytoplasm in astroglial processes of the severe case. These findings are consistent with previous reports of increased reactive astroglial processes paralleling severity in MTLE (Eid et al., 2008; Jabs et al., 2008; Krishnan et al., 1994; Mathern et al., 1997; Mitchell et al., 1999; Van Paesschen et al., 1997). Other neurological diseases also show alterations in gross astroglial morphology and glial dysfunction (Binder and Steinhauser, 2006; Lee et al., 2006; Matute et al., 2006; Tian et al., 2005; Wetherington et al., 2008), while more subtle changes in the amount of astroglia accompany spine fluctuations during estrus, long-term potentiation, and kindling in the hippocampus (Hawrylak et al., 1993; Lam and Leranth, 2003; Wenzel et al., 1991) and during environmental enrichment and motor learning in visual and motor cortices (Jones and Greenough, 2002). In normal rat hippocampus, glutamate transporters can be found in perisynaptic neuronal membranes (Chen et al., 2002), but they are most highly concentrated along astroglial membranes (Bergles and Jahr, 1998; Chaudhry et al., 1995; Lehre and Danbolt, 1998). Thus, elevated glutamate transport and less

extracellular glutamate might be expected with progressive astroglial processes during MTLE.

Glutamate transporters have been detected in astroglial processes in sclerotic hippocampus (Bjornsen et al., 2007; Eid et al., 2004), but their numbers are reduced (Mathern et al., 1999; Proper et al., 2002). Furthermore, despite the widespread loss of neurons and synapses, glutamate receptors are increased in epileptic hippocampus (Brines et al., 1997; Matute et al., 2006; Seifert et al., 2004). In addition, extracellular glutamate concentration is higher than normal in epileptic hippocampus (Cavus et al., 2005; During and Spencer, 1993). Perhaps the expanded astroglial surface area results in a lower density of glutamate transporters (Bjornsen et al., 2007) and more glutamate receptors to respond to the elevated concentration of extracellular glutamate.

Astroglia communicate by calcium signaling through gap junctions (Cornell-Bell and Finkbeiner, 1991; Dani et al., 1992; Verkhratsky and Kettenmann, 1996). Upregulation of gap junction proteins has been associated with reactive astroglial processes in MTLE (Fonseca et al., 2002). We discovered specialized junctions between astroglial processes, which occurred more frequently in the moderate than the mild case. If these specialized junctions are astroglial gap junctions, then elevated calcium signaling between astroglia could facilitate release of glutamate from the astroglia (Eid et al., 2008; Fellin et al., 2006; Montana et al., 2006; Tian et al., 2005) and might contribute to glutamate excitotoxicity during MTLE.

### Perisynaptic Astroglia Occur at Larger Human Hippocampal Synapses

Astroglial processes also function to preserve and eliminate synapses. Secretion of thrombospondin and cholesterol from neighboring astroglia facilitates synaptogenesis in tissue culture (Christopherson et al., 2005; Mauch et al., 2001). Contact with perisynaptic astroglia promotes structural integrity, persistence, and efficacy of synapses (Hama et al., 2004; Piontek et al., 2002; Schuster et al., 2001; Spacek and Harris, 1998). Conversely, astroglial secretion of complement cascade proteins protects strong synapses, but punishes smaller competing synapses and results in appropriate synapse elimination (Stevens et al., 2007). The absence of interdigitating astroglial processes might help to explain why multiple synapses could form on a single spine in the absence of the “punishing” effect of complement cascade.

We found perisynaptic astroglia at ~40–45% of the human hippocampal synapses in the mild to moderate cases, which compares to ~60% of normal adult rat hippocampal synapses (Ventura and Harris, 1999; Witcher et al., 2007). Whether this represents a significant decrease resulting from prior epileptic seizures or a difference between rat and human hippocampus will require more study.

In both rat and human hippocampus, larger synapses were more likely to have some perisynaptic astroglia

and the degree to which synapses were surrounded by astroglial processes decreased proportionately with increasing synapse size, thus leaving much of the perimeter open and susceptible to spillover of substances at larger synapses (Ventura and Harris, 1999; Witcher et al. 2007). Astroglial uptake of extracellular glutamate can be impaired during epilepsy (Cavus et al., 2005; Proper et al., 2002). However, if enough glutamate can be transported away there may be a neuroprotective effect of perisynaptic astroglia (Harris and Rosenberg, 1993; Rosenberg and Aizenman, 1989). In addition, the astroglia-free distances between neighboring synapses were greater in the moderate than the mild condition, which might ameliorate the effects of spill over. Thus, synapse specificity may have been preserved in the mild case by the perisynaptic astroglia and in the moderate case by diffusion distances. In contrast, synapses on individual multisynaptic spines in the severe case had no intervening astroglia; hence, they might have shared neurotransmitters and had compromised input specificity among the many axons that synapsed on each of them.

### CONCLUDING REMARKS

Three-dimensional reconstruction of hippocampal synapses revealed similarities between the rat model system and humans. The human cases with mild or moderate histopathology had intractable epileptic seizures that were cured by removal of their hippocampus. Nevertheless, the synapses in the surgical specimens were similar to normal adult rat hippocampus in morphology, composition, and degree of association with perisynaptic astroglia. The case with severe histopathology was also cured of seizures by removal of the hippocampus, but the few synapses remaining in this surgical specimen were highly aberrant, showing multisynaptic spines and loss of synapse-specific associations with perisynaptic astroglia. More work of this nature will be needed to determine which forms of MTLE or other seizure disorders destroy synapses and whether perisynaptic astroglia might be targeted to restore synaptic function in human hippocampus.

### ACKNOWLEDGMENTS

We thank Deborah Ard, Neetu Bali, Kimberly Smith, Elizabeth Perry, and Robert Smith for technical assistance; Dr. John Fiala for the RECONSTRUCT™ software; Dr. Ioulia Fomitcheva for developing Informed Consents and Assents Documents and maintaining the study according to the FDA guidelines. We thank Cameron Slayden for assistance with spine reconstructions and Andrew Swift for illustrating Figs. 2e and 6d. We thank Drs. Josef Spacek and Richard Hessler for assistance in initially interpreting pathologic state of resected hippocampi. We thank Drs. Paul Biddinger and Michael Boyd for their support with the Aperio Scan

Scope System. We thank Drs. Almira Vazdarjanova and Lynnette McCluskey for reviewing an early draft of this manuscript and Dr. Dan Johnston for his helpful comments.

### REFERENCES

- Andrioli A, Alonso-Nanclares L, Arellano JI, DeFelipe J. 2007. Quantitative analysis of parvalbumin-immunoreactive cells in the human epileptic hippocampus. *Neuroscience* 149:131–143.
- Arellano JI, Munoz A, Ballesteros-Yanez I, Sola RG, DeFelipe J. 2004. Histopathology and reorganization of chandelier cells in the human epileptic sclerotic hippocampus. *Brain* 127:45–64.
- Baloyannis SJ, Kim SU. 1979. Experimental modification of cerebellar development in tissue culture: X-Irradiation induces granular degeneration and unattached purkinje cell dendritic spines. *Neurosci Lett* 12:283–288.
- Bergles DE, Jahr CE. 1998. Glial contribution to glutamate uptake at Schaffer collateral–commissural synapses in the hippocampus. *J Neurosci* 18:7709–7716.
- Binder DK, Steinhauser C. 2006. Functional changes in astroglial cells in epilepsy. *Glia* 54:358–368.
- Bjornsen LP, Eid T, Holmseth S, Danbolt NC, Spencer DD, de Lanerolle NC. 2007. Changes in glial glutamate transporters in human epileptogenic hippocampus: Inadequate explanation for high extracellular glutamate during seizures. *Neurobiol Dis* 25:319–330.
- Blumcke I, Pauli E, Clusmann H, Schramm J, Becker A, Elger C, Merschhemke M, Meencke HJ, Lehmann T, von Deimling A, Scheiwe C, Zentner J, Volk B, Romstock J, Stefan H, Hildebrandt M. 2007. A new clinico-pathological classification system for mesial temporal sclerosis. *Acta Neuropathol* 113:235–244.
- Brines ML, Sundaresan S, Spencer DD, Lanerolle NC. 1997. Quantitative autoradiographic analysis of ionotropic glutamate receptor subtypes in human temporal lobe epilepsy: Up-regulation in reorganized epileptogenic hippocampus. *Eur J Neurosci* 9:2035–2044.
- Bushong EA, Martone ME, Ellisman MH. 2004. Maturation of astrocyte morphology and the establishment of astrocyte domains during postnatal hippocampal development. *Int J Dev Neurosci* 22:73–86.
- Bushong EA, Martone ME, Jones YZ, Ellisman MH. 2002. Protoplasmic astrocytes in CA1 stratum radiatum occupy separate anatomical domains. *J Neurosci* 22:183–192.
- Cavus I, Kasoff WS, Cassaday MP, Jacob R, Gueorguieva R, Sherwin RS, Krystal JH, Spencer DD, Abi-Saab WM. 2005. Extracellular metabolites in the cortex and hippocampus of epileptic patients. *Ann Neurol* 57:226–235.
- Chaudhry FA, Lehre KP, van Lookeren C, Ottersen OP, Danbolt NC, Storm-Mathisen J. 1995. Glutamate transporters in glial plasma membranes: Highly differentiated localizations revealed by quantitative ultrastructural immunocytochemistry. *Neuron* 15:711–720.
- Chen S, Hillman DE. 1982. Plasticity of the parallel fiber-purkinje cell synapse by spine takeover and new synapse formation in the adult rat. *Brain Res* 240:205–220.
- Chen W, Aoki C, Mahadomrongkul V, Gruber CE, Wang GJ, Blitzblau R, Irwin N, Rosenberg PA. 2002. Expression of a variant form of the glutamate transporter GLT1 in neuronal cultures and in neurons and astrocytes in the rat brain. *J Neurosci* 22:2142–2152.
- Christopherson KS, Ullian EM, Stokes CC, Mullen CE, Hell JW, Agah A, Lawler J, Mosher DF, Bornstein P, Barres BA. 2005. Thrombospondins are astrocyte-secreted proteins that promote CNS synaptogenesis. *Cell* 120:421–433.
- Cornell-Bell AH, Finkbeiner SM. 1991. Ca<sup>2+</sup> waves in astrocytes. *Cell Calcium* 12:185–204.
- Dani JW, Chernjavsky A, Smith SJ. 1992. Neuronal activity triggers calcium waves in hippocampal astrocyte networks. *Neuron* 8:429–440.
- During MJ, Spencer DD. 1993. Extracellular hippocampal glutamate and spontaneous seizure in the conscious human brain. *Lancet* 341:1607–1610.
- Eid T, Thomas MJ, Spencer DD, Runden-Pran E, Lai JCK, Malthankar GV, Kim JH, Danbolt NC, Ottersen OP, de Lanerolle NC. 2004. Loss of glutamine synthetase in the human epileptogenic hippocampus: Possible mechanism for raised extracellular glutamate in mesial temporal lobe epilepsy. *Lancet* 363:28–37.
- Eid T, Williamson A, Lee TS, Petroff OA, de Lanerolle NC. 2008. Glutamate and astrocytes—Key players in human mesial temporal lobe epilepsy? *Epilepsia* 49 Suppl 2:42–52.
- Fellin T, Gomez-Gonzalo M, Gobbo S, Carmignoto G, Haydon PG. 2006. Astrocytic glutamate is not necessary for the generation of

- epileptiform neuronal activity in hippocampal slices. *J Neurosci* 26:9312–9322.
- Fiala JC. 2005. Reconstruct: A free editor for serial section microscopy. *J Microsc* 218:52–61.
- Fiala JC, Harris KM. 2001a. Cylindrical diameters method for calibrating section thickness in serial electron microscopy. *J Microsc* 202:468–472.
- Fiala JC, Harris KM. 2001b. Extending unbiased stereology of brain ultrastructure to three-dimensional volumes. *J Am Med Inform Assoc* 8:1–16.
- Fiala JC, Kirov SA, Feinberg MD, Petrak LJ, George P, Goddard CA, Harris KM. 2003. Timing of neuronal and glial ultrastructure disruption during brain slice preparation and recovery in vitro. *J Comp Neurol* 465:90–103.
- Fiala JC, Spacek J, Harris KM. 2002. Dendritic spine pathology: Cause or consequence of neurological disorders? *Brain Res Brain Res Rev* 39:29–54.
- Fonseca CG, Green CR, Nicholson LF. 2002. Upregulation in astrocytic connexin 43 gap junction levels may exacerbate generalized seizures in mesial temporal lobe epilepsy. *Brain Res* 929:105–116.
- Hama H, Hara C, Yamaguchi K, Miyawaki A. 2004. PKC signaling mediates global enhancement of excitatory synaptogenesis in neurons triggered by local contact with astrocytes. *Neuron* 41:405–415.
- Harris KM, Jensen FE, Tsao B. 1992. Three-dimensional structure of dendritic spines and synapses in rat hippocampus (CA1) at postnatal day 15 and adult ages: Implications for the maturation of synaptic physiology and long-term potentiation. *J Neurosci* 12:2685–2705.
- Harris KM, Perry E, Bourne J, Feinberg M, Ostroff L, Hurlburt J. 2006. Uniform serial sectioning for transmission electron microscopy. *J Neurosci* 26:12101–12103.
- Harris KM, Rosenberg PA. 1993. Localization of synapses in rat cortical cultures. *Neuroscience* 53:495–508.
- Harris KM, Stevens JK. 1989. Dendritic spines of CA1 pyramidal cells in the rat hippocampus: Serial electron microscopy with reference to their biophysical characteristics. *J Neurosci* 9:2982–2997.
- Harris KM, Sultan P. 1995. Variation in number, location, and size of synaptic vesicles provides an anatomical basis for the non-uniform probability of release at hippocampal CA1 synapses. *J Neuropharmacol* 34:1387–1395.
- Hawrylak N, Chang FL, Greenough WT. 1993. Astrocytic and synaptic response to kindling in hippocampal subfield CA1. II. Synaptogenesis and astrocytic process increases to in vivo kindling. *Brain Res* 603:309–316.
- Henze DA, McMahon DB, Harris KM, Barrionuevo G. 2002. Giant miniature EPSCs at the hippocampal mossy fiber to CA3 pyramidal cell synapse are monoquantal. *J Neurophysiol* 87:15–29.
- Jabs R, Seifert G, Steinhauser C. 2008. Astrocytic function and its alteration in the epileptic brain. *Epilepsia* 49 Suppl 2:3–12.
- Jensen FE, Harris KM. 1989. Preservation of neuronal ultrastructure in hippocampal slices using rapid microwave-enhanced fixation. *J Neurosci Methods* 29:217–230.
- Jiang M, Lee CL, Smith KL, Swann JW. 1998. Spine loss and other persistent alterations of hippocampal pyramidal cell dendrites in a model of early-onset epilepsy. *J Neurosci* 18:8356–8368.
- Jones TA, Greenough WT. 2002. Behavioral experience-dependent plasticity of glial-neuronal interactions. In: Volterra A, Magistretti PJ, Haydon PG, editors. *The tripartite synapse: Glia in synaptic transmission*. Oxford: Oxford University Press. pp 248–265.
- Kirov SA, Petrak LJ, Fiala JC, Harris KM. 2004. Dendritic spines disappear with chilling but proliferate excessively upon rewarming of mature hippocampus. *Neuroscience* 127:69–80.
- Kirov SA, Sorra KE, Harris KM. 1999. Slices have more synapses than perfusion-fixed hippocampus from both young and mature rats. *J Neurosci* 19:2876–2886.
- Krishnan B, Armstrong DL, Grossman RG, Zhu ZQ, Rutecki PA, Mizrahi EM. 1994. Glial cell nuclear hypertrophy in complex partial seizures. *J Neuropathol Exp Neurol* 53:502–507.
- Lam TT, Leranath C. 2003. Gonadal hormones act extrinsic to the hippocampus to influence the density of hippocampal astroglial processes. *Neuroscience* 116:491–498.
- Lee TS, Bjornsen LP, Paz C, Kim JH, Spencer SS, Spencer DD, Eid T, de Lanerolle NC. 2006. GAT1 and GAT3 expression are differentially localized in the human epileptogenic hippocampus. *Acta Neuropathol (Berl)* 111:351–363.
- Lehre KP, Danbolt NC. 1998. The number of glutamate transporter subtype molecules at glutamatergic synapses: Chemical and stereological quantification in young adult rat brain. *J Neurosci* 18:8751–8757.
- Leranath C, Shanabrough M, Redmond DE Jr. 2002. Gonadal hormones are responsible for maintaining the integrity of spine synapses in the CA1 hippocampal subfield of female nonhuman primates. *J Comp Neurol* 447:34–42.
- Lisman J, Harris KM. 1993. Quantal analysis and synaptic anatomy—Integrating two views of hippocampal plasticity. *Trends Neurosci* 16:141–147.
- Lisman J, Harris KM. 1994. Who's been nibbling on my PSD: Is it LTD? *J Physiol (Paris)* 88:193–195.
- Mathern GW, Babb TL, Armstrong D. 1997. Hippocampal sclerosis. In: Engel JJ, Pedley TA, editors. *Epilepsy: A comprehensive textbook*. Philadelphia: Lippincott-Raven. pp 133–154.
- Mathern GW, Mendoza D, Lozada A, Pretorius JK, Dehnes Y, Danbolt NC, Nelson N, Leite JP, Chimelli L, Born DE, Sakamoto AC, Assirati JA, Fried I, Peacock WJ, Ojemann GA, Adelson PD. 1999. Hippocampal GABA and glutamate transporter immunoreactivity in patients with temporal lobe epilepsy. *Neurology* 52:453–472.
- Matute C, Domercq M, Sanchez-Gomez MV. 2006. Glutamate-mediated glial injury: Mechanisms and clinical importance. *Glia* 53:212–224.
- Mauch DH, Nagler K, Schumacher S, Goritz C, Muller EC, Otto A, Pfrieger FW. 2001. CNS synaptogenesis promoted by glia-derived cholesterol. *Science* 294:1354–1357.
- Mazzanti M, Haydon PG. 2003. Astrocytes selectively enhance N-type calcium current in hippocampal neurons. *Glia* 41:128–136.
- Megias M, Emri Z, Freund TF, Gulyas AI. 2001. Total number and distribution of inhibitory and excitatory synapses on hippocampal CA1 pyramidal cells. *Neuroscience* 102:527–540.
- Mitchell LA, Jackson GD, Kalnins RM, Saling MM, Fitt GJ, Ashpole RD, Berkovic SF. 1999. Anterior temporal abnormality in temporal lobe epilepsy: A quantitative MRI, histopathologic study. *Neurology* 52:327–336.
- Montana V, Malarkey EB, Verderio C, Matteoli M, Parpura V. 2006. Vesicular transmitter release from astrocytes. *Glia* 54:700–715.
- Multani P, Myers RH, Blume HW, Schomer DL, Sotrel A. 1994. Neocortical dendritic pathology in human partial epilepsy: A quantitative Golgi study. *Epilepsia* 35:728–736.
- Murai KK, Nguyen LN, Irie F, Yamaguchi Y, Pasquale EB. 2003. Control of hippocampal dendritic spine morphology through ephrin-A3/EphA4 signaling. *Nat Neurosci* 6:153–160.
- Parnavelas JG, Lynch G, Brecha N, Cotman C, Globus A. 1974. Spine loss and regrowth in hippocampus following deafferentation. *Nature* 248:71–73.
- Paul LA, Scheibel AB. 1986. Structural substrates of epilepsy. *Adv Neurol* 44:775–786.
- Pfrieger FW, Barres BA. 1997. Synaptic efficacy enhanced by glial cells in vitro. *Science* 277:1684–1687.
- Piontek J, Regnier-Vigouroux A, Brandt R. 2002. Contact with astroglial membranes induces axonal and dendritic growth of human CNS model neurons and affects the distribution of the growth-associated proteins MAP1B and GAP43. *J Neurosci Res* 67:471–483.
- Proper EA, Hoogland G, Kappen SM, Jansen GH, Rensen MG, Schrama LH, van Veelen CW, van Rijen PC, van Nieuwenhuizen O, Gispén WH, de Graan PN. 2002. Distribution of glutamate transporters in the hippocampus of patients with pharmaco-resistant temporal lobe epilepsy. *Brain* 125:32–43.
- Raisman G, Field PM. 1973. A quantitative investigation of the development of collateral reinnervation after partial deafferentation of the septal nuclei. *Brain Res* 50:241–264.
- Rosenberg PA, Aizenman E. 1989. Hundred-fold increase in neuronal vulnerability to glutamate toxicity in astrocyte-poor cultures of rat cerebral cortex. *Neurosci Lett* 103:162–168.
- Rosset A, Spadola L, Ratib O. 2004. OsiriX: An open-source software for navigating in multidimensional DICOM images. *J Digit Imaging* 17:205–216.
- Scheibel AB, Scheibel ME. 1977. Specific postnatal threats to brain development: Dendritic changes. In: Berenberg SR, editor. *Brain: Fetal and infant: Current research on normal and abnormal development*. The Hague, Netherlands: Martinus Nijhoff Medical Division. pp 302–315.
- Schuster T, Krug M, Stalder M, Hackel N, Gerardy-Schahn R, Schachner M. 2001. Immunoelectron microscopic localization of the neural recognition molecules L1, NCAM, and its isoform NCAM180, the NCAM-associated polysialic acid, beta1 integrin and the extracellular matrix molecule tenascin-R in synapses of the adult rat hippocampus. *J Neurobiol* 49:142–158.
- Seifert G, Huttmann K, Schramm J, Steinhauser C. 2004. Enhanced relative expression of glutamate receptor 1 flip AMPA receptor subunits in hippocampal astrocytes of epilepsy patients with Ammon's horn sclerosis. *J Neurosci* 24:1996–2003.
- Spacek J, Harris KM. 1998. Three-dimensional organization of cell adhesion junctions at synapses and dendritic spines in area CA1 of the rat hippocampus. *J Comp Neurol* 393:58–68.
- Spencer SS. 2002. When should temporal-lobe epilepsy be treated surgically? *Lancet Neurol* 1:375–382.
- Stevens B, Allen NJ, Vazquez LE, Howell GR, Christopherson KS, Nouri N, Micheva KD, Mehalow AK, Huberman AD, Stafford B, Sher

- A, Litke AM, Lambris JD, Smith SJ, John SW, Barres BA. 2007. The classical complement cascade mediates CNS synapse elimination. *Cell* 131:1164–1178.
- Swann JW, Al Noori S, Jiang M, Lee CL. 2000. Spine loss and other dendritic abnormalities in epilepsy. *Hippocampus* 10:617–625.
- Tian GF, Azmi H, Takano T, Xu Q, Peng W, Lin J, Oberheim N, Lou N, Wang X, Zielke HR, Kang J, Nedergaard M. 2005. An astrocytic basis of epilepsy. *Nat Med* 11:973–981.
- Van Paesschen W, Revesz T, Duncan JS, King MD, Connelly A. 1997. Quantitative neuropathology and quantitative magnetic resonance imaging of the hippocampus in temporal lobe epilepsy. *Ann Neurol* 42:756–766.
- Ventura R, Harris KM. 1999. Three-dimensional relationships between hippocampal synapses and astrocytes. *J Neurosci* 19:6897–6906.
- Verkhratsky A, Kettenmann H. 1996. Calcium signalling in glial cells. *Trends Neurosci* 19:346–352.
- Wenzel J, Lammert G, Meyer U, Krug M. 1991. The influence of long-term potentiation on the spatial relationship between astrocyte processes and potentiated synapses in the dentate gyrus neuropil of rat brain. *Brain Res* 560:122–131.
- West MJ, Coleman PD, Flood DG. 1988. Estimating the number of granule cells in the dentate gyrus with the disector. *Brain Res* 448:167–172.
- Wetherington J, Serrano G, Dingledine R. 2008. Astrocytes in the epileptic brain. *Neuron* 58:168–178.
- Witcher MR, Kirov SA, Harris KM. 2007. Plasticity of perisynaptic astroglia during synaptogenesis in the mature rat hippocampus. *Glia* 55:13–23.
- Woolley CS, McEwen BS. 1992. Estradiol mediates fluctuation in hippocampal synapse density during the estrous cycle in the adult rat. *J Neurosci* 12:2549–2554. Erratum in: *J Neurosci* 1992 Oct;12(10):following table of contents.
- Woolley CS, Wenzel HJ, Schwartzkroin PA. 1996. Estradiol increases the frequency of multiple synapse boutons in the hippocampal CA1 region of the adult female rat. *J Comp Neurol* 373:108–117.
- Xu-Friedman MA, Harris KM, Regehr WG. 2001. Three-dimensional comparison of ultrastructural characteristics at depressing and facilitating synapses onto cerebellar Purkinje cells. *J Neurosci* 21:6666–6672.